Journal of Engineering and Applied Science

RESEARCH

Open Access

Preparation of inorganic catalysts from ceramic industry wastes for use in the production of biofuel

Sarah Hisham Hassan[1*], Nahed Kamal Attia[1], Guzine Ibrahim El Diwani[1], Reem Sayed Ettouney[2], Mahmoud Abdel Hakim El-Rifai[2] and Shereen Kamel Amin[1]

*Correspondence:
sarahhisham85@gmail.com

[1] Chemical Engineering and Pilot Plant Department, National Research Centre (NRC), Cairo, Dokki, Egypt
[2] Chemical Engineering Department, Faculty of Engineering, Cairo University, Giza, Egypt

Abstract

Catalysts' surface structural features and characterizations play an important role in many chemical industrial processes among which is biofuel production. Heterogeneous catalysts strongly affect the types of products in catalytic hydrocracking of oils. The present study aims at the preparation of low-cost inorganic catalysts with improved catalytic activity. This will then be used in the production of bio-jet fuel — conforming to ASTM specifications — by hydrocracking of *Jatropha* oil. Five types of inorganic catalysts have been prepared and tested. The best results were obtained from the catalyst produced from ceramic wastes. It produced the highest bio-jet yield (51%) and the highest freezing point (− 52 °C). A BET surface area of 21.9 m^2/g and a "total pore volume" of 0.025877 cm^3/g were obtained.

Keywords: Inorganic heterogeneous catalysis, Egyptian ceramic industry, Waste recycling, *Jatropha* oil, Bio-jet fuel, Biofuel, Hydrocracking

Introduction

The catalytic hydrocracking process is used to convert feedstocks such as recycled cooking greases, animal fats, and plant oils to biofuels such as biogasoline, bio-jet, biodiesel, and mazot [1, 2]. Catalysts are classified as homogeneous, heterogeneous, and biocatalysts. Each catalyst is produced by different manufacturing methods [3]. The catalytic conversion processes take place under pressurized H_2 and in a temperature range of 280–450 °C. The product types, yield, and selectivity are controlled by the choice of catalyst [4, 5].

The catalyst properties are controlled by the pore shape, acidity, and size. There is a wide range of different types of catalysts such as macroporous (silica-alumina, alumina), mesoporous (MCM-41 and SBA-15), microporous (zeolite), composite microporous-mesoporous [1–3], Ni/ZSM-5 [6], CoMo/Al_2O_3, Ni-HZSM-5/SBA-15 [7], Ni–Mo/Al_2O_3 [8] and Ni–W/SiO_2–Al_2O_3, PdNi/HZSM-5 catalyst [9], NiMo/SA-2 and NiMo/Z-10, CoMo/MCM-41 [10], K-modified zeolite ZSM-5 [11], mesoporous-alumina-supported CoMo catalysts [10], Ni/H-Beta [8], Ni/SAPO-11 [12], and ZSM-5-Zn [13].

In heterogeneous catalysis, the catalytic reaction mechanism takes place according to the following steps [14]: reactant diffuses to the surface, adsorption inside the catalyst surface, surface diffusion of reactants, reaction occurs on the surface, surface diffusion of products, products desorption from the surface, and diffusion away from the surface [15].

There is a direct correlation between the availability of catalytic sites on the catalyst surface and the number of reactant molecules that have been transformed into products during a certain time [8]. The active sites are maximized by the high surface area obtained from porous oxide particles (carriers) such as Al_2O_3, SiO_2, TiO_2, SiO_2-Al_2O_3, or combinations, activated carbon [3, 14], and spread of the catalytic components such as Rh, Fe, PdO, Pd, Pt, CuO, CoO, and Ni onto the catalyst surface. Generally, the catalytic body is formed by the combination of two parts, the support and the precursor [16, 17]. The support could be organic, inorganic and modified. Examples of the support include NH4Y, ZSM-5, SAPO-11, Zeolite β, Bentonite P-140, SAPO-34, ZSM-5, SBA-15, and MCM-41 [3, 18]. The precursor is a solution of either a metal salt or complex containing Cr, Rh, Mn, Fe, Cu, Co, Ru, Ni, Zn, etc. [3] Ni (NO_3) $2.6H_2$. Typical solutions include $RuCl_3.3H_2O$, "Ca $(NO_3)_2.4H_2O$" and "La $(NO_3)_3.6H_2O$", "Al $(NO_3)_3.9H_2O$", and "Zn $(NO_3)_2.4H_2O$," etc. [3].

Catalyst preparation techniques include surface modification such as acid, basic, or heat treatment of clays [19–22] and preparation by chemical reaction of pure components and materials such as the production of "ultra-stable Y zeolite USY" [23], Hβ [24], HZSM-5 [10], HZSM-5 catalysts Si/AL ratio 198 [18], titania, zirconia, ceria, loaded on supports such as amorphous alumino-silicate and nano γ-Al2O3 alumina catalyst [25].

The present work aims to preparation of a low-cost inorganic catalyst from ceramic industries wastes to be used in the bio-jet fuel production, which is conforming to ASTM specification by hydrocracking of *Jatropha* oil. In order to the objectives of economic, environmental, and also to achieve sustainable development, saves sources of raw materials for future generations.

Methods

Materials

Imported bentonite (C) obtained from Geohellas — technical clays, Natural Solutions, Greece, initially developed for the edible oil refining sector.

Egyptian bentonite (B) was obtained from Borg El Arab, Alexandria, Egypt. It comes from Egyptian quarries and is generally used for the manufacture of ceramics, pottery, and handicrafts.

Three different ceramics industrial wastes obtained from Ceramica Alfa factory, 6th of October City, are used as catalysts after modification. The wastes are the kiln rollers hazardous fine waste (W_1), which is a high alumina waste obtained from the surface grinding of kiln rollers, ceramics floor dust (W_2), and wall dust (W_3).

Hydrochloric acid was purchased from Sigma-Aldrich Laborchemikalien GmbH Company, Germany. The acid concentration is 37%, and its molecular weight is 36.5.

Jatropha oil was obtained from solid–liquid extraction of *Jatropha curcas* seeds at National Research Center, Egypt.

Catalyst preparation

Each catalyst is prepared by adding 50 g of bentonite clays (B, C) and ceramics wastes (W_1, W_2, W_3) to 500 ml of 0.1-M HCl, and the mixture is fed to a round flask connected to a condenser and heated to 110 °C, for 4 h. The resulting suspensions are then rapidly quenched in 500-ml ice-cold distilled water. After quenching, the suspension was filtered and washed several times using distilled water until chloride ions are completely removed. The modified clays and wastes are then dried in an oven at 110 °C and calcinated at 550 °C for 4 h.

Catalysts and materials characterization

- X-ray fluorescence spectrometry (XRF) analyses were carried out on an Axios, PANalytical 2005, and wavelength-dispersive x-ray fluorescence (WD-XRF) sequential spectrometer. X-ray diffraction (XRD) tests to confirm the crystal structure were carried out with "the following settings:" goniometer = theta/theta; minimum step size 2 theta: 0.0001; minimum step size omega: 0.0001", sample stage = stage for flat samples/holders, diffractometer system = Empyrean, and anode material: Cu. The scans were taken at $2\theta = 4–80°$.
- Fourier transform infrared spectroscopy (FTIR) analysis was performed using Origin Jasco Infrared Spectrum (FT/IR-6100 type A) over the wave number range 4000–399 cm^{-1}.
- The surface area of the inorganic catalysts and raw materials was studied using version 1.21 of the Quantachrome TouchWin™ to determine the Brunauer, Emmett, and Teller (BET) surface area. Before the experiments, all material samples were degassed at 200 °C for 6 h. The "BET"-specific surface area was estimated from the linear part of the adsorption curve. "The total pore volumes of micro- and mesopores were directly obtained from nitrogen adsorption at P/PO around (0.1–0.98)". "The pore diameter distribution was calculated from the desorption branch using" "Barrett-Joyner-Haleda (BJH) formula (Berraaouan et al., 2020; Hussin et al., 2011; Ro & Novakovi, 2010)". It is important to ensure that the purity of the adsorptive is not less than 99.999%. In addition, the accuracy of the results depends on careful preparation and sampling of the adsorbent (Thommes et al., 2015).
- Particle size distributions (PSD) of the raw material samples were measured using Particle Sizing Systems, Inc., Santa Barbara, USA, and intensity-weighted Gaussian distribution analysis method for solid particles. Some PSD of raw material samples were measured using laboratory cumulative screen analysis apparatus. Scanning electron microscopy (SEM) and energy dispersive X-ray analyses (EDX), carried out on Quanta 250 FEG (field emission gun) attached with EDX unit, were used to examine the microstructure of the produced prepared catalyst. Scanning the microstructure and the surface of the specimen can be done by accelerating a beam of fine focused electron under maximum potential difference of 30 kV. Using a magnification 14 × up to 1,000,000, microstructure is then photographed. The prepared catalyst samples were coated with gold layer (thickness 200 to 300 A^o) using K550X sputter coater equipment and then examined under SEM.

Biofuel preparation

The procedure of the laboratory preparation of the biofuel involves the following steps. *Jatropha* oil is filtered, and 100 g of the filtrate is fed to the stainless-steel laboratory batch reactor operated for 18 min at a hydrogen gas pressure of 4 bar and a temperature range of 350–450 °C. The collected product is fractionated in a laboratory distillation unit to obtain the following products corresponding to the distillation temperature range: bio-gasoline (60–170 °C), bio-jet fuel (170–270 °C), bio-diesel (270–330 °C), and Mazot and tar at higher temperatures.

Biofuel specification

The freezing point of bio-jet fuel samples is measured according to ASTM specifications. A total of 15 ml from every sample are placed in a glass tube under liquid nitrogen until the sample totally freezes. The freezing point was measured by reading the thermometer indicated at the last thin crystal layer in the solid–liquid mixture. Existent gum content according to ASTM D-381 of jet fuel must not exceed 7 mg/100 ml [21]. The gum values are estimated for the Jet A-1 blended with 5% vol. bio-jet fuel.

Results and discussion

X-ray fluorescence

Table 1 shows that the XRF analyses of the natural clays and ceramics wastes are almost the same. It is obvious that SiO_2 and Al_2O_3 are the major components of all raw materials and prepared catalysts, with trace amounts of other metal oxides. The hydrochloric acid effect on raw materials is to increase the silica content and to decrease the abundance of metal oxides such as CaO, Na_2O, Fe_2O_3, MnO, Ca^{2+}, and Na^{+} cations, which dissolve readily by mild acid treatment. These oxides exist at interlayer of exchangeable cations. Although Fe^{3+}, Al^{3+}, and Mg^{2+} cations belong to the octahedral sheet inside the clay structure, they impede acid attack. The rise within the relative percentage content of the insoluble Si^{4+} cations happens as a result of a reduction of the opposite cations

Table 1 XRF analysis of raw and prepared catalysts

Main constituents	wt%									
	C	M-C	B	M-B	W_1	M-W_1	W_2	M-W_2	W_3	M-W_3
SiO_2	48.91	51.69	48.70	67.17	23.55	21.24	61.13	72.62	62.29	70.51
TiO_2	0.10	0.25	1.20	1.58	0.33	0.26	0.98	0.64	0.74	0.95
Al_2O_3	2.80	1.22	19.19	19.75	63.86	68.29	20.82	17.04	14.67	19.21
Fe_2O_3tot	20.10	33.62	9.55	5.42	1.16	1.60	3.66	1.27	2.8	2.74
MnO	0.247	0.13	0.10	0.01	–	0.03	0.031	0.01	0.023	0.02
MgO	14.37	3.67	2.06	0.87	1.96	1.82	1.37	0.79	0.32	0.34
CaO	0.49	0.39	4.47	0.35	3.51	0.29	1.4	0.42	8.26	0.30
Na_2O	0.06	0.04	1.37	0.57	0.8	0.29	2.96	3.43	1.60	1.76
K_2O	0.09	0.08	1.19	1.53	0.48	0.17	1.52	2.38	2.14	2.29
P_2O_5	0.02	0.03	0.25	0.10	0.17	0.08	0.2	0.05	0.14	0.10
SO_3	0.03	0.06	1.28	0.09	–	0.04	0.4	0.06	0.44	0.07
Cl	0.03	0.08	0.44	0.02	–	0.02	0.08	0.02	0.07	0.021
LOI	11.47	6.64	9.96	2.32	–	0.24	5.26	1.09	7.37	1.50

from the octahedral and interlayer sheets [19, 22, 26]. As a result, the hydronium cations introduced into the interlayer spacing of the clay maintain the layer structure. It was reported that the clay activated using sulfuric acid shows a significant increase in L.O.I and SO^{3-} percentages as well as a reduction in alumina and silica percentages. This happens initially by replacement of the interlayer cations with H^{+} ions from the sulfuric acid, thus causing dissolution of structural cations (Al^{3+}, Si^{4+}). The specific surface area of the clay thus increases as a result of the dealumination of the clay structure [19, 22, 25]. It was also reported that the clay activated using phosphoric acid shows an increase in the SiO_2 percentage as a result of the reduction of the opposite cations from the interlayer and octahedral sheets [27], and a high P_2O_5 percentage has been noticed.

X-ray diffraction

The X-ray diffraction (XRD) spectra of natural clays (C and B), the acid-activated clays used as catalysts in this study (MC and MB), ceramics wastes (W_1, W_2, and W3), and prepared catalysts (MW_1, MW_2, MW_3) are presented in Figs. 1 and 2. The clays and ceramic wastes seem to be well crystallized. It is seen that treatment with HCl modifies the peaks of ceramic wastes and clays. The peaks illustrate the intensity and width of all prepared catalysts, which are nearly identical to the pure raw materials. This indicates structural preservation. The peak severity is an index of the degree of laminar structure retained by the clay [19, 22, 28, 29].

The XRD analysis of imported clay shown in Fig. 1 reveals that it consists of 24.5% SiO_2 and 75.5% gmelinite. The XRD analysis of the imported clay after modification consists of 96.6% monalbite and 3.4% zeolite. Egyptian clays XRD analysis shown in Fig. 1

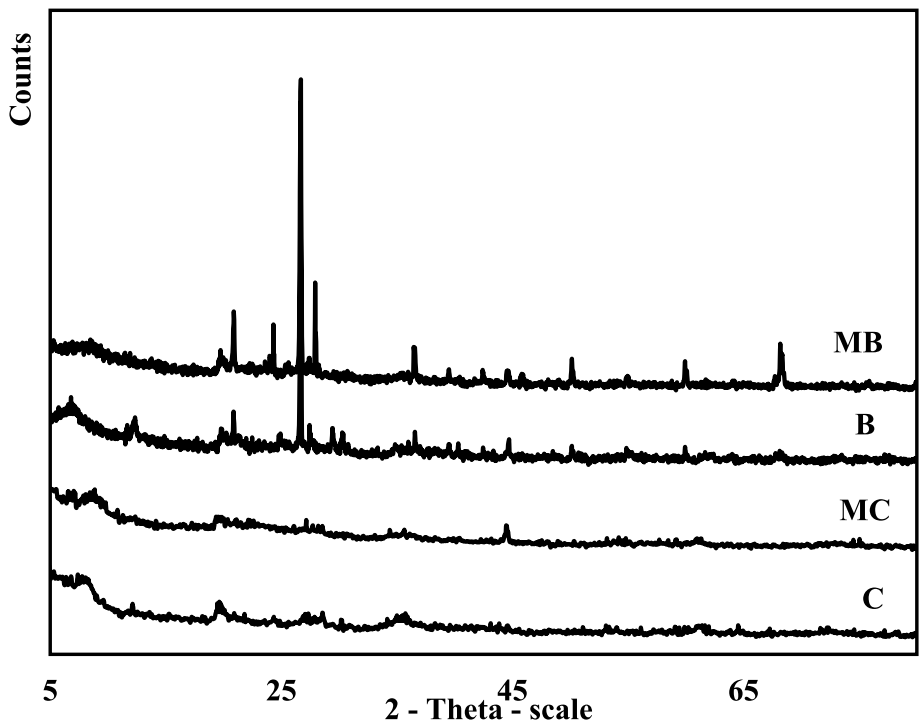

Fig. 1 XRD pattern for imported and Egyptian bentonite (C, MC, B, and MB)

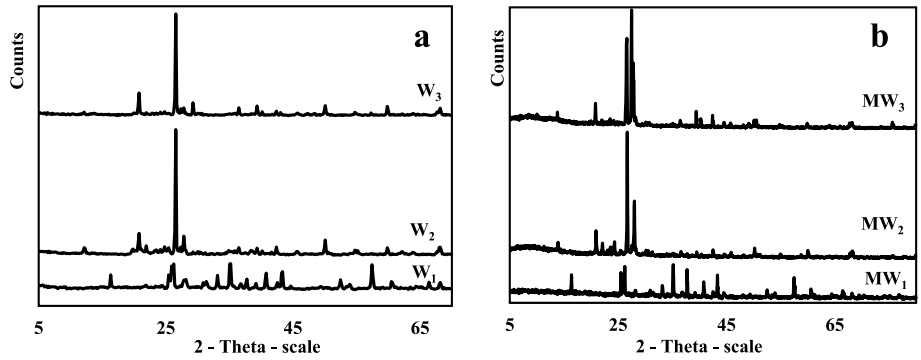

Fig. 2 XRD pattern for ceramic industrial wastes. **a** before modification and **b** after modification

Table 2 FTIR wave number of the catalyst

Band	C	MC	B	MB	W_1	MW_1	W_2	MW_2	W_3	MW_3
1	3426	3441	3397	3425	3429	3432	3440	3440	3418	3435
2	2927	–	2930	2927	–	–	–	–	2928	2925
3	–	–	2840	2853	–	–	–	–	2852	–
4	–	–	1741	–	–	–	–	–	1742	–
5	1644	1632	1646	1644	1632	1632	1632	1631	1645	1639
6	–	–	1456	–	–	–	–	–	–	–
7	–	–	–	–	1176	1177	–	–	–	–
8	–	–	–	–	–	–	–	1086	–	–
8	1024	1048	1028	1025	–	–	1033	1040	1025	1037
9	–	798	–	–	724	–	781	780	–	776
10	671	–	–	–	–	–	–	–	–	–
11	–	–	–	–	595	593	–	–	–	–
12	–	–	–	–	–	–	536	530	538	536
13	–	–	–	472	–	–	466	463	468	462
14	446	452	–	–	454	454	–	–	–	–

indicates that it consists mainly of 44.3% kaolinite and 34.1% quartz. The prepared catalysts from the Egyptian clays contain 62.5% quartz and 17.2% sodium aluminum silicate as shown in Fig. 1. The XRD analysis shown in Fig. 2a indicates that the ceramics waste W_1 is composed mainly of mullite and corundum. The ceramic waste, W_2, mainly consists of albite, kaolinite, and microcline, while W_3 is mostly microcline, albite, calcite, and quartz. The prepared catalyst from ceramics wastes MW_1 contains 33.9% corundum and 51.8% mullite as seen in Fig. 2b; MW_2 contains 20.6% aluminum silicate hydroxide, 35% albite low, and 40.3% microcline, and MW_3 contains 16.6% microcline, 36.3% albite, and 47.1% quartz low.

Fourier transform infrared spectroscopy

The infrared spectral analysis of imported and Egyptians clays is shown in Fig. 11 and Table 2. The imported clays contain wave numbers of 3426, 2927, 1644, 1024, and 671 cm^{-1} as seen from Table 2, H–O-H stretching of absorbed water, C–H stretching, OH stretching hydration, and Si–O stretching of clay minerals, respectively. For the prepared catalyst MC, the wave numbers of 3441, 1632, 1048, and 798 cm^{-1} appear which

corresponds to H–O-H stretching of absorbed water, OH stretching hydration, Si–O stretching, and Si–O quartz, respectively.

The Egyptian clays contain wave numbers of 3397, 2930, 1646, and 1028 cm^{-1}) as seen in Table 2 which indicate H–O-H stretching of absorbed water, C–H stretching, and OH stretching and hydration of clay minerals, respectively. The prepared catalyst MB shows wave numbers of 3425, 2927, 1644, 1025, and 472 cm^{-1} due to H–O-H stretching of absorbed water, C–H stretching, OH stretching hydration, Si–O stretching, and Si–O-Si bending, respectively, which accounts for the bending and stretching vibrations of the hydroxyl groups OH found in water molecules absorbed on the surface of the Egyptian clay. This is due to the loss of hydroxyl OH groups and molecules of water by the elimination of octahedral cations, which are attached to the framework of Egyptian clay [22, 25]. After the Egyptian clay was modified with hydrochloric acid, the amorphous Si–O-Si units were formed in three-dimensional networks. This is indicated by the rise of the wave number 472 cm^{-1}. The infrared spectral analysis of the ceramic wastes and their prepared catalysts are shown in Fig. 3 and Table 2. It is seen that their behavior is similar to that of clays.

The FTIR wave numbers of W_1 and MW_1 are 3429, 1632, and 724 cm^{-1} and 3429, 3432, and 1632 cm^{-1}, respectively, referring to H–O-H stretching of the absorbed water and Si–O quartz. The FTIR wave numbers for W_2 and MW_2 are 3440, 1631, 1033, 781, 536, and 466 cm^{-1} and 3440, 1631, 1040, 780, 580, and 463 cm^{-1} revealing H–O-H stretching of absorbed water, OH stretching hydration, Si–O stretching, Si–O quartz, Fe–O, Fe_2O_3 Si–O-Al stretching, and Si–O-Si bending, respectively. This indicates the partial solubility of Al, Fe, and Mg cations in the structure of bentonite clay. The FTIR wave numbers for W_3 and MW_3 are 3418, 2928, 1645, 1025, 538, and 468 cm^{-1} and 3435, 2925, 1639, 1037, 776, 536, and 462 cm^{-1} indicating H–O-H stretching of absorbed water, C–H stretching, OH stretching hydration, Si–O stretching, Si–O quartz, Fe–O, Fe_2O_3 Si–O-Al stretching, and Si–O-Si bending, respectively [5, 30–34].

N_2 physisorption

The results of the BET surface area, N_2-adsorption–desorption analysis, and BJH pore size distribution of the raw clays, ceramic wastes, and the prepared catalyst samples are shown in Figs. 4, 5, 6, 7, 8 and in Table 3. In all samples, a sharp

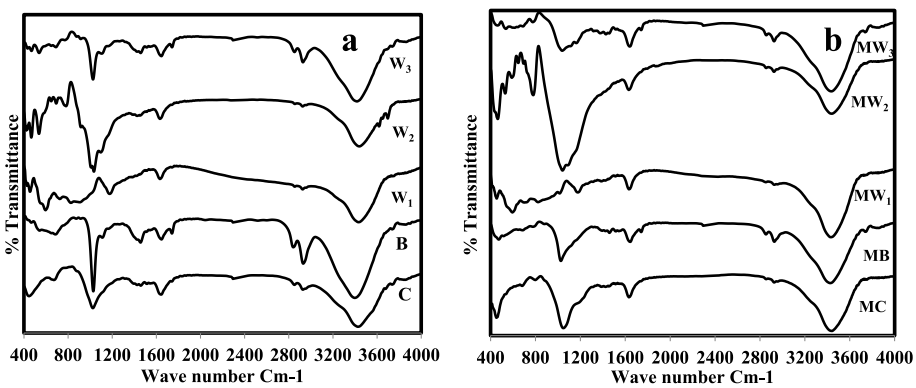

Fig. 3 FTIR pattern for ceramic industrial waste, imported "and" Egyptian. **a** before modification and **b** after modification

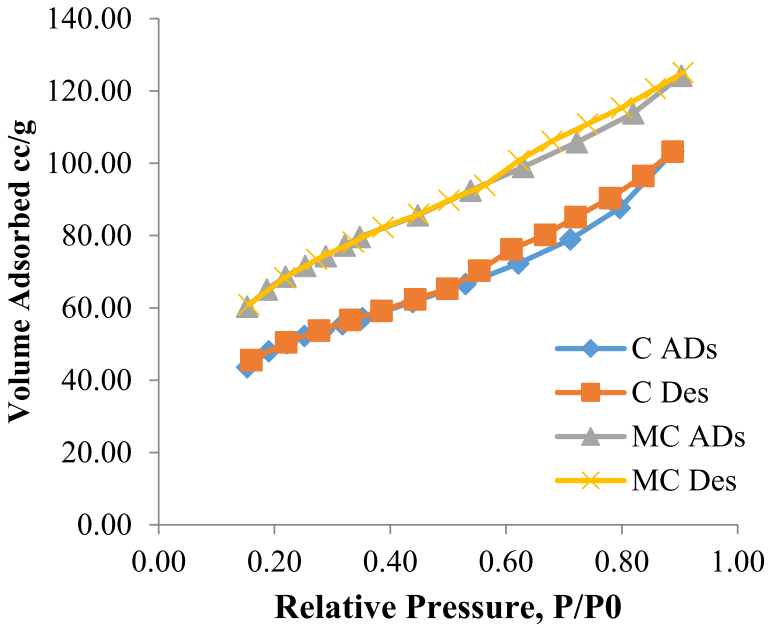

Fig. 4 Adsorption–desorption isotherm of C and MC

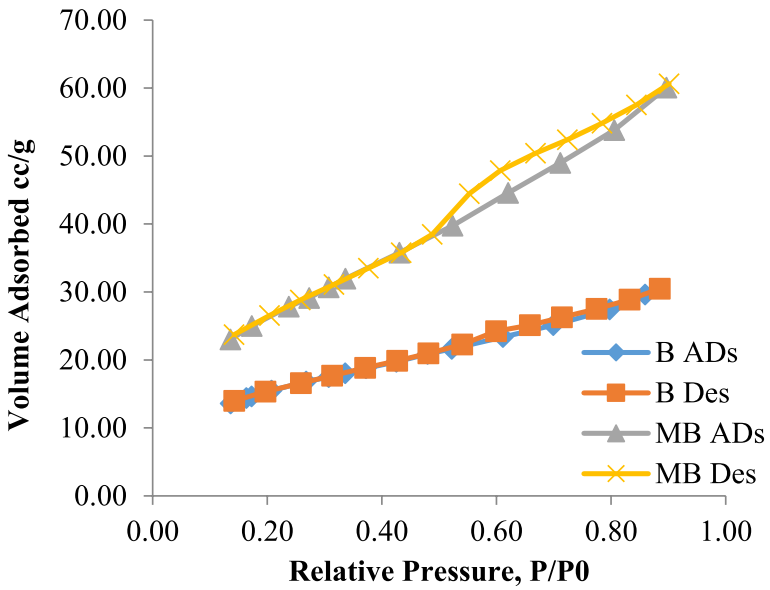

Fig. 5 Adsorption–desorption isotherm of B and MB

inflection appears in the prepared catalysts on increasing total pore volume, average pore diameter, and BET surface area. The large surface area and pore volume of catalysts increase the rate of the reactions. MW_3 has the largest surface area in industrial ceramics wastes, and the surface area of MC is larger than that of MB. From these results, it can be concluded that MW_3 and MC catalysts have the best heterogeneous catalytic action. The observe BJH pore size distribution values show that for the prepared catalysts, the pore size increased with a wide range of distribution.

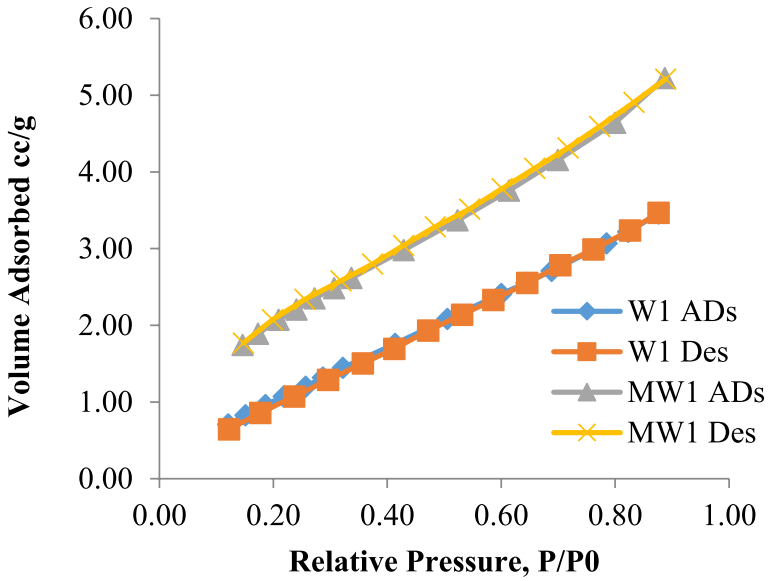

Fig. 6 Adsorption–desorption isotherm of W_1 and MW_1

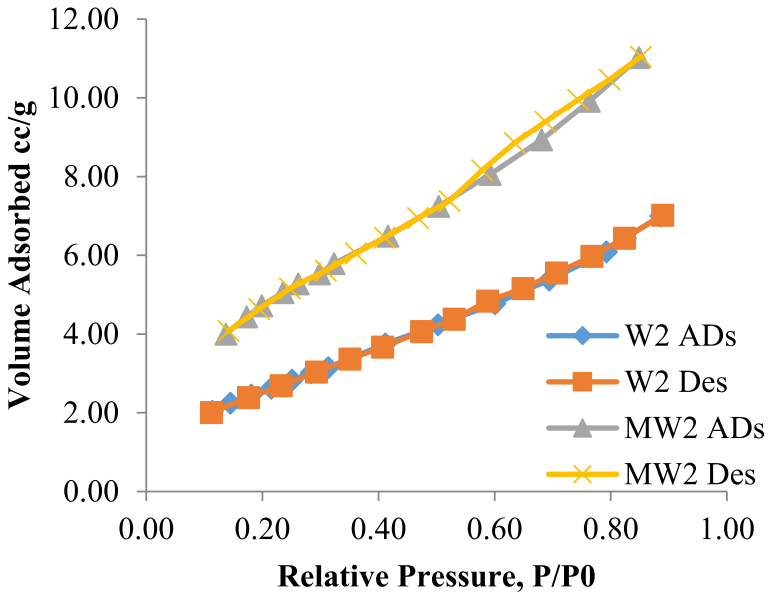

Fig. 7 Adsorption–desorption isotherm of W_2 and MW_2

This indicates good reactant distribution during the catalytic process. The adsorption–desorption isotherm curves of the prepared catalysts are shown in Figs. 4, 5, 6, 7 and 8. It is seen that the modified catalysts have higher capability of reactant adsorption and product desorption at their surface. The MC catalyst has the highest adsorption–desorption isotherm and is followed by MB and MW_3, respectively.

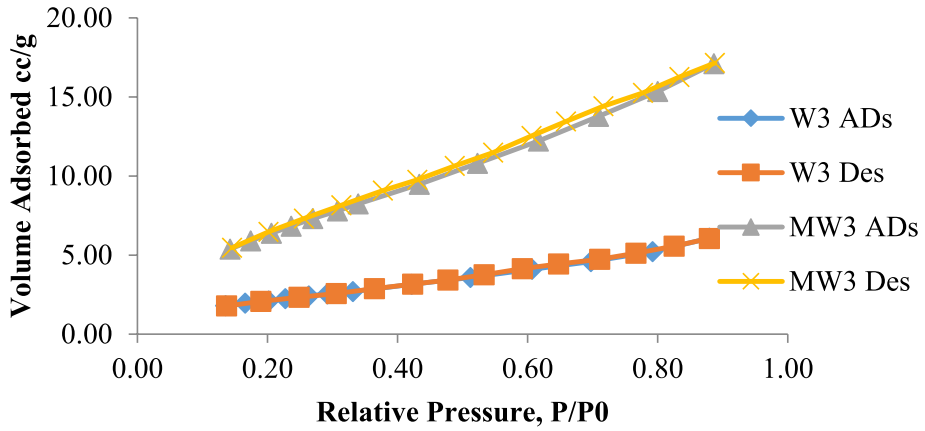

Fig. 8 Adsorption–desorption isotherm of W_3 and MW_3

Table 3 Specific surface area, pore diameter, and pore volume of raw materials and prepared inorganic catalysts

Sample name	Molecular weight (g/mol)	Cross-section area (A^2/mol)	Total pore volume (cm^3/g)	S_{BET} (m^2/g)	Average pore diameter (nm)
C	28.013	16.2	0.17317	171.885	4.03
MC	28.013	16.2	0.22211	264.104	3.364
B	28.013	16.2	0.048352	52.2959	3.6984
MB	28.013	16.2	0.10388	96.2112	4.3186
W_1	28.013	16.2	0.0059396	5.63346	4.2174
MW_1	28.013	16.2	0.0083937	7.46664	4.4966
W_2	28.013	16.2	0.011772	8.86131	5.3138
MW_2	28.013	16.2	0.017188	16.2807	4.223
W_3	28.013	16.2	0.010331	7.98942	5.1722
MW_3	28.013	16.2	0.025877	21.8616	4.7346

Particle size distributions

The cumulative particle size analyses of Egyptian bentonite and prepared catalyst MB are measured. It is clear that the raw bentonite and MB are very fine powders having a mean diameter of 453.5 nm and 2746 nm, respectively. Also, the particle size distribution of the MB is practically larger than B; this may be due to the degree of catalyst grinding after its laboratory preparations.

SEM and EDX

The SEM scan and EDX analysis of the surface of the representative samples during the catalytic hydrocracking process are presented below. The first sample is the MW_3 catalyst and solid remaining in the reactor after reaction shown in Fig. 9. The second sample represents MW_3 catalyst and is shown in Fig. 10. The EDX of the sample is displayed in Table 4. It is seen that the sample mainly contains carbon atoms indicating that the catalyst may be covered with coke and mazot.

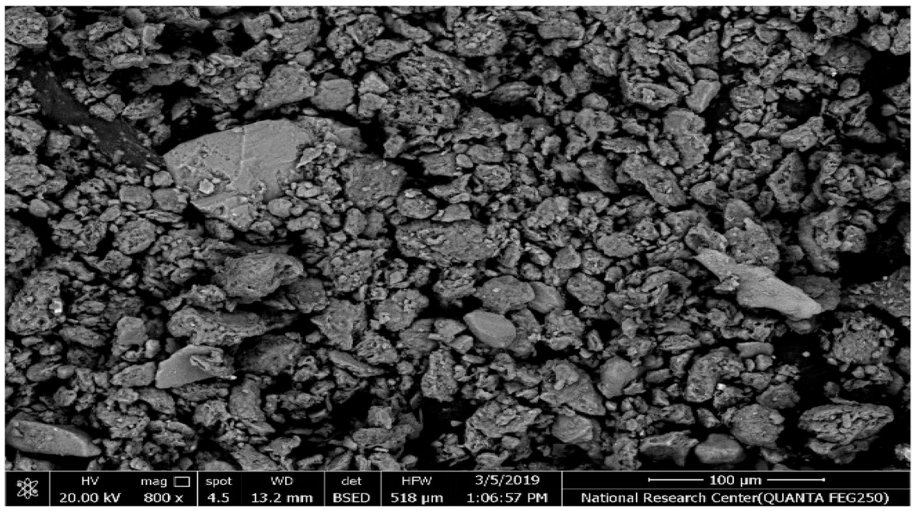

Fig. 9 SEM of MW_3 catalyst and solid remaining in reactor after reaction

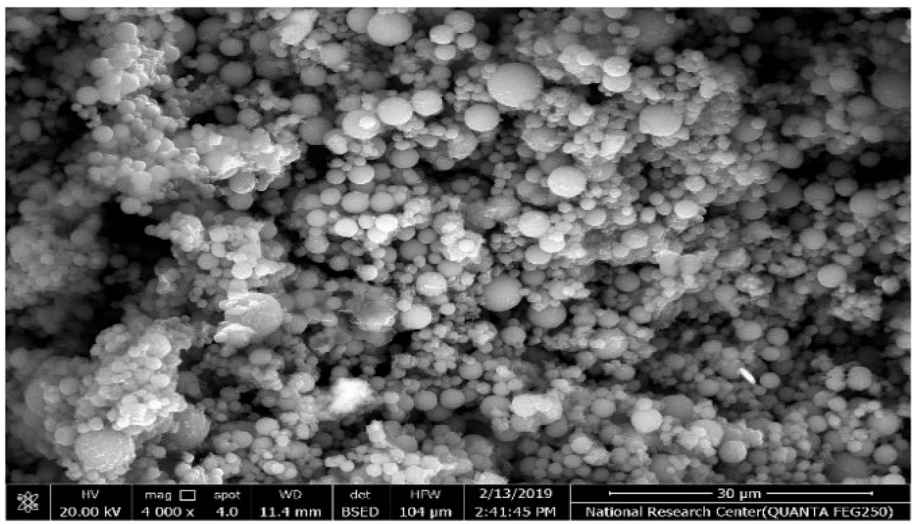

Fig. 10 SEM of MW_3 catalyst after biofuel filtrations

Table 4 EDX of MW_3 catalyst

Element	Weight %	Atomic %
C K	87.27	90.14
N K	1.49	1.32
O K	10.76	8.35
Si K	0.11	0.05
P K	0.2	0.08
S K	0.18	0.07

Bio-jet fuel

The five catalysts were used in the production of bio-jet fuel by catalytic hydrocracking of *Jatropha* oil under the obtained optimum operating conditions of 350 °C, 4 bar

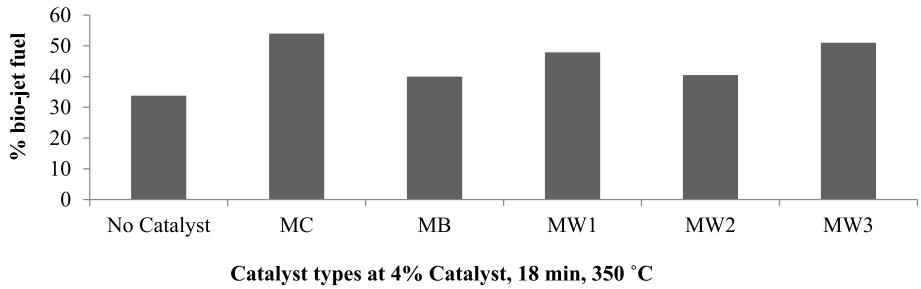

Fig. 11 Types of catalyst effect on yield of bio-jet fuel production

Table 5 The mixture of (5% bio-jet with 95% jet A-1) fuel specifications

Catalyst type	No. — catalyst	4% MC	4% MB	4% MW_1	4% MW_2	4% MW_3
Freezing point (°C)	− 52	− 51	− 51	− 48	− 48	− 56
Existent gum mg/100 ml	6.4	5.9	6.1	6	6.2	5.9

H_2, 18 min reaction time, and 4% catalyst. The biofuel mixture that was obtained from the reaction was separated in a distillation tower into four fractions: biogasoline, bio-jet, biodiesel, and mazot according to their boiling points. Figure 11 shows that the bio-jet fuel yield increased from 34 to 54% when using the different prepared catalysts. The optimum yield was obtained using MC (54%) followed by MW_3 (51%) and MW_1 (48%) with the lowest yield achieved by MB (40%). The bio-jet fuels produced using the different catalysts were tested, and their specifications are shown in Table 5 that conformed to the ASTM specifications of the freezing point (− 47 °C to − 56 °C) and existent gum content (5.9–6.4 mg/100 ml).

Preliminary techno-economic evaluation of MW_3 catalyst preparation

The preliminary techno-economic evaluation was carried out on MW_3 catalyst at a consumption capacity of 1183 t/year. It is assumed that the plant will operate for 7200 h, and the bio-jet fuel plant capacity is assumed to be 10,000 ton/year.

The purchased cost and specifications of all equipment that were obtained from the market are shown in Tables 6 and 7. The total purchased cost of equipment was calculated at US $403,500. The total capital cost presented in Table 8 was found to be US $2.19 MM/year. The annual production cost summarized in Table 9 was US $1.44 MM/year. Accordingly, the production cost of MW_3 catalyst was calculated as US $1214/t.

It is to be noted that the price of the prepared inorganic catalyst MW_3 is lower than other known catalysts used in the catalytic hydrocracking of *Jatropha* oil to produce bio-jet fuel, US $18 per BBL of the produced bio-jet fuel. The price was compared with the Pt/C, Ni/Al_2O_3 catalysts price of US $23,589/t, and US $26,014/t, respectively, which was obtained in the previous study of Precommercial heterogeneous catalyst price: a simple step-based method [35]. The difference in the price is due to the fact that the MW_3 is an industrial waste and has no value. Not only is the MW_3 catalyst easy to produce but also this does not require the necessity of recycling, given that it is from industrial waste and

Table 6 Equipment sizing of inorganic catalyst production

Equipment	Calculated capacity	Operating conditions	Market survey capacity	Market survey specification	Ref
CSTR reactor	4.2 ton	110 °C, 4 h	5000 l	• Motor power 15 kw • Stirring speed 63/85 r/min • Inner pot size 1800 mm	Laizhou Taihe Chemical Machinery Co
Heat exchanger	4.2 ton	Inlet: 80 °C Outlet: 30 °C	Max 50 m^3/h	• Shell and tube heat exchanger • Power 2.2–400	Wuxi New Wuhuan Energy Saving Technology Co
Centrifugal solid–liquid washing & separator	0.2 ton/h	Free Cl^- ions	Productivity 8–15 m^3/h	• Rotation speed 4000 r.p.m • Moisture content 20% • Power 22 kw	Xiangtan County Centrifuge Plant Co
Rotary dryer	0.2 ton/h	100 °C	Volume 7.85 m^3	• Speed 3–7 r/min • Power 4 kw • Model • (D × L, m): 1 × 10	Gongyi Derui Machinery Co., Ltd
Rotary kiln	1.2 ton	550 °C, 4 h	1–40 t/h	• (D × L, m): 1.9 × 26 • Power 18.5–550	Henan Zhengzhou Mining Machinery Co
Ball mill grinding	0.2 ton/h	Nanoparticle	Volume 0.4 m^3	• Power 18.5 kw • D, L (m): 0.9, 0.9	Qixia Dali Mine Machinery Co

Table 7 Equipment purchased cost of catalyst production

Equipment cost	US $/unit	Total US $
CSTR reactor (4 reactors)	50,000	200,000
Heat exchanger (4 heat exchangers)	2000	8000
Centrifuge	30,000	30,000
Rotary dryer	70,000	70,000
Rotary kiln	80,000	80,000
Grinder	15,500	15,500
PCE (equipment purchased cost)		403,500

is widely available daily, and its recovery needs more than one step, which is costly. As a preliminary assessment, the bio-jet fuel production cost will be lower if MW_3 is used as the catalyst instead of the other prepared commercial heterogeneous catalyst in the catalytic hydrocracking process.

Conclusions

Acid modifications that applied to all raw materials are as follows: 0.1-M HCl, heated to 110 °C, for 4 h and calcination at 550 °C for 4 h. It was necessary to generate the catalytic activity. Five types of catalysts and their raw materials are characterized and tested by XRF, XRD, FTIR, SEM, EDX, and BET. All prepared inorganic catalysts performed efficiently during catalytic hydrocracking of *Jatropha* oil to produce biofuel, operated for

Table 8 Total capital cost of catalyst production

Cost		US $
Installation	0.45 PCE	181,575
Piping	0.45 PCE	181,575
Instrumentation	0.15 PCE	60,525
Electrical	0.1 PCE	40,350
Building	0.1 PCE	40,350
Utilities	0.375 PCE	151,313
Storage	0.2 PCE	80,700
Site development	0.05 PCE	20,175
Ancillary buildings	0.225 PCE	90,787.5
PPC (A) (physical plant cost)		1,250,850
Fees of contractor	"0.050 PPC"	62,542.5
Engineering & design	"0.250 PPC"	312,713
"Contingency"	"0.10 PPC"	125,085
(B)		500,340
FCI (fixed capital cost)		1751,190
TCI (total capital cost)		2,188,988

Table 9 Production cost of catalyst

Variable direct cost				
Raw material	**US $/ton**	**Ton/y**	**US $/y**	**Ref**
HCL	150	1623.57	243,535.896	Horizon Chemical for Special Chemicals Company
Ceramics industrial waste	0	1648.3	0	
Utilities	US $/kw or m^3	Kw or m^3/year	US $/y	Ref
Water (m^3/year)	0.530	141,803	75,231.25059	Ministry of Housing, Utilities & Urban Communities
Electricity (kw/year)	0.0617	1317,600	81,381.17647	Electricity Regulatory Authority and Consumer Protection Regulatory Authority
Miscellaneous	10% of maintenance		17,511.9	
Total			417,660.2238	
Fixed direct cost				
Labor, 15 men/shift, 3 shift, 2118 $/year (man)			95,294.11765	
Plant overhead	"(0.50 × labor)"		47,647.05882	
Supervision	"(0.20 × labor)"		19,058.82353	
Overhead	"(0.150 × FCI)"		262,678.5	
Rent	"(0.010 × FCI)"		17,511.9	
Interest	"(0.020 × FCI)"		35,023.8	
Maintenance	"(0.10 × FCI)"		175,119	
Insurance	"(0.010 × FCI)"		17,511.9	
Royalties	"(0.010 × FCI)"		17,511.9	
Total			687,357	
Indirect cost				
• Research and development • General overheads • Sales & distribution	0.3 direct manufacturing cost		331,505.1671	
Annual production cost			1,436,522.391	
Production cost of catalyst ($/ton)			1214	

18 min, 4 bar H_2, and temperature range (350 –450 °C), which was then separated by fractional distillation into biogasoline, bio-jet fuel, and biodiesel with a residue of mazot and coke.

The produced biofuel components were separated, tested, and were found to conform to the ASTM jet fuel specifications. The MW_3 is produced the highest bio-jet yield (51%) and the highest freezing point (− 52 °C). A "BET surface area" of 21.9 m^2/g and a "total pore volume" of 0.0258 cm^3/g were obtained.

A preliminary techno-economic assessment for the production of bio-jet fuel using MW_3 catalyst revealed that the catalyst had a price of US $1214/t. This indicates that the bio-jet fuels produced using MW_3 catalyst are more economical and conform to the ASTM specifications when compared to the other prepared commercial heterogeneous catalyst Pt/C and Ni/Al_2O_3 that had a price of US $23,589/t and US $26,014/t, respectively.

Abbreviations

ASTM	American Society for Testing and Materials
B	Egyptian bentonite
C	Imported bentonite
CASE	Cold acid solvent extraction
CO	Carbon monoxide
CO_2	Carbon dioxide
CSTR	Continues stirred tank reactor
D	Diameter
EPA	Environmental Protection Agency
FCI	Fixed cost investment
FTIR	Fourier transform infrared spectroscopy
GHG	Greenhouse gas
H	Height
H_2	Hydrogen
KOH	Potassium hydroxide
kW	Kilowatt
L	Length
MB	Modified Egyptian bentonite
MC	Modified Imported bentonite
MW_1	Modified $waste_1$
MW_2	Modified $waste_2$
MW_3	Modified $waste_3$
NO_x	Nitrogen oxides
PCE	Equipment purchased cost
PPC	Physical plant cost
r	Radius
r/min	Revolutions per minute
RKF	Runge–Kutta–Fehlberg
SO_x	Sulfur oxides
TCI	Total capital investment
USA	United States of America
W_1	$Waste_1$
W_2	$Waste_2$
W_3	$Waste_3$
WHSV	Weight hourly space velocity
V	Volume
XRD	X-ray powder diffraction
XRF	X-ray fluorescence
τ	Residence time

Acknowledgements

Authors would like to express their sincere gratitude to the National Research Center in Egypt for its invaluable support throughout experimental work and chemical analysis. It is funded by the National Research Centre award number (6/3/18).

Authors' contributions

SH, writing the paper and doing the experimental work in catalyst preparation and production of biofuel, catalyst characterizations, and biofuel specification. GI,reviews the paper, interprets biofuel results, and develops the working

plan. NK, participating in the experimental work of the bio-jet fuel, analyzing data results, and writing and review the paper. SK, interpretation of catalyst results and review the paper. MR and RS, review the paper. All authors have read and approved the manuscript and ensure that this is the case.

Funding
National Research Centre, award number (6/3/18), grant recipient master degree of Sarah Hisham Hassan.

Availability of data and materials
Not applicable in this section.

Declarations

Ethics approval and consent to participate
Not applicable in this section.

Consent for publication
Not applicable in this section.

Competing interests
The authors declare that they have no competing interests.

Received: 15 March 2023 Accepted: 17 June 2023
Published online: 28 June 2023

References

1. Taufiqurrahmi N, Bhatia S (2011) Catalytic cracking of edible and non-edible oils for the production of biofuels. Energy Environ Sci 4(4):1087–1112. https://doi.org/10.1039/c0ee00460j
2. Velusamy K, Devanand J, Senthil Kumar P, Soundarajan K, Sivasubramanian V, Sindhu J, Vo DVN (2021) A review on nano-catalysts and biochar-based catalysts for biofuel production. Fuel 306(May):121632. https://doi.org/10.1016/j.fuel.2021.121632
3. Shahinuzzaman M, Yaakob Z, Ahmed Y (2017) Non-sulphide zeolite catalyst for bio-jet-fuel conversion. Renew Sustain Energy Rev 77(January):1375–1384. https://doi.org/10.1016/j.rser.2017.01.162
4. Lei X, Xin H, Du X, Yang H, Zeng Y, Zhou L, Juan C, Zhang H, Li D, Hu C (2022) Efficiency conversion of jatropha oil into high-quality biofuel over the innovative Ni-Mo2N based catalyst. Fuel 324(PB):124548. https://doi.org/10.1016/j.fuel.2022.124548
5. Utami, M., Setiawan, P., Izul Falah, I., Suheryanto, Shidiq, M., Wijaya, K., Jarin, T., Sumathijones, C., Abd- Elkader, O. H., O H Abd-Elkader, M., Woong Chang, S., & Ravindran, B. (2022). Synthesis of biodiesel from castor oil catalyzed by sodium hydroxide dispersed on bentonite. Sustainable Energy Technologies and Assessments, 53(PB), 102526. https://doi.org/10.1016/j.seta.2022.102526.
6. Shi N, Liu QY, Jiang T, Wang TJ, Ma LL, Zhang Q, Zhang XH (2012) Hydrodeoxygenation of vegetable oils to liquid alkane fuels over Ni/HZSM-5 catalysts: methyl hexadecanoate as the model compound. Catal Commun 20:80–84. https://doi.org/10.1016/j.catcom.2012.01.007
7. Weng Y, Qiu S, Ma L, Liu Q, Ding M, Zhang Q, Zhang Q, Wang T (2015) Jet-fuel range hydrocarbons from biomass-derived sorbitol over Ni-HZSM-5/SBA-15 catalyst. Catalysts 5(4):2147–2160. https://doi.org/10.3390/catal5042147
8. Yu F, Zhang C, Geng R, Zhou H, Dong Q, Liu S, Fan B, Li R (2023) Hydrocracking of naphthalene over beta zeolite coupled with NiMo/γ-Al2O3: investigation of metal and acid balance based on the composition of industrial hydrocracking catalyst. Fuel 344(2022):128049. https://doi.org/10.1016/j.fuel.2023.128049
9. Zhang J, Zhao C (2015) A new approach for bio-jet fuel generation from palm oil and limonene in the absence of hydrogen. Chem Commun 51(97):17249–17252. https://doi.org/10.1039/c5cc06601h
10. Ooi XY, Gao W, Ong HC, Lee HV, Juan JC, Chen WH, Lee KT (2019) Overview on catalytic deoxygenation for biofuel synthesis using metal oxide supported catalysts. Renew Sustain Energy Rev 112(June):834–852. https://doi.org/10.1016/j.rser.2019.06.031
11. Lang L, Zhao S, Yin X, Yang W, Wu C (2015) Catalytic activities of K-modified zeolite ZSM-5 supported rhodium catalysts in low-temperature steam reforming of bioethanol. Int J Hydrogen Energy 40(32):9924–9934. https://doi.org/10.1016/j.ijhydene.2015.06.016
12. Zuo H, Liu Q, Wang T, Ma L, Zhang Q, Zhang Q (2012) Hydrodeoxygenation of methyl palmitate over supported ni catalysts for diesel-like fuel production. Energy Fuels 26(6):3747–3755. https://doi.org/10.1021/ef300063b
13. Zhao X, Wei L, Cheng S, Huang Y, Yu Y, Julson J (2015) Catalytic cracking of camelina oil for hydrocarbon biofuel over ZSM-5-Zn catalyst. Fuel Process Technol 139:117–126. https://doi.org/10.1016/j.fuproc.2015.07.033
14. Hagemeyer, A., & Clara, S. (2016). Materials : Catalysts $. Reference Module in Materials Science and Materials Engineering, March 2015, 1–8. https://doi.org/10.1016/B978-0-12-803581-8.01121-8.
15. Trisunaryanti W, Wijaya K, Triyono T, Wahyuningtyas N, Utami SP, Larasati S (2022) Characteristics of coconut shell-based activated carbon as Ni and Pt catalyst supports for hydrotreating Calophyllum inophyllum oil into hydrocarbon-based biofuel. J Environ Chem Eng 10(5):108209. https://doi.org/10.1016/j.jece.2022.108209
16. Kazakov MO, Smirnova MY, Dubinin ME, Bogomolova TS, Dik PP, Golubev IS, Revyakin ME, Klimov OV, Noskov AS (2023) Combining USY and ZSM-23 in Pt / zeolite hydrocracking catalyst to produce diesel and lube base oil with improved cold flow properties. Fuel 344(December 2022):128085. https://doi.org/10.1016/j.fuel.2023.128085
17. Milovanović, B., Marinović, S., Vuković, Z., Milutinović-Nikolić, A., Petrović, R., Banković, P., & Mudrinić, T. (2022). The influence of cobalt loading on electrocatalytic performance toward glucose oxidation of pillared

montmorillonite-supported cobalt. Journal of Electroanalytical Chemistry, 915(April). https://doi.org/10.1016/j.jelechem.2022.116332
18. Sirajudin N, Jusoff K, Yani S, Ifa L, Roesyadi A (2013) Biofuel production from catalytic cracking of palm oil. World Appl Sci J 26(26):67–71. https://doi.org/10.5829/idosi.wasj.2013.26.nrrdsi.26012
19. Elfadly AM, Zeid IF, Yehia FZ, Abouelela MM, Rabie AM (2017) Production of aromatic hydrocarbons from catalytic pyrolysis of lignin over acid-activated bentonite clay. Fuel Process Technol 163(May):1–7. https://doi.org/10.1016/j.fuproc.2017.03.033
20. Hussin F, Aroua MK, Mohd W, Wan A (2011) Textural characteristics, surface chemistry and activation of bleaching earth : a review. Chem Eng J 170(1):90–106. https://doi.org/10.1016/j.cej.2011.03.065
21. Ismail A, Mansour SA, Yossif MA, Bekhit M, Negm NA (2018) Production of jet biofuels from catalytic cracking of vegetable oils using acidic catalysts. Curr J Appl Sci Technol 27(4):1–9. https://doi.org/10.9734/CJAST/2018/41162
22. Rabie AM, Mohammed EA, Negm NA (2018) Feasibility of modified bentonite as acidic heterogeneous catalyst in low temperature catalytic cracking process of biofuel production from nonedible vegetable oils. J Mol Liq 254(March):260–266. https://doi.org/10.1016/j.molliq.2018.01.110
23. Zheng Q, Huo L, Li H, Mi S, Li X, Zhu X, Deng X, Shen B (2017) Exploring structural features of USY zeolite in the catalytic cracking of Jatropha curcas L. seed oil towards higher gasoline/diesel yield and lower CO2emission. Fuel 202:563–571. https://doi.org/10.1016/j.fuel.2017.04.073
24. Ramya G, Sivakumar T, Arif M, Ahmed Z (2015) Catalytic cracking using an Hβ catalyst for the production of green fuel: optimization studies. Energy Sources, Part A: Recovery, Utilization and Environmental Effects 37(7):758–765. https://doi.org/10.1080/15567036.2011.594862
25. Negm NA, Rabie AM, Mohammed EA (2018) Molecular interaction of heterogeneous catalyst in catalytic cracking process of vegetable oils: chromatographic and biofuel performance investigation. Appl Catal B 239:36–45. https://doi.org/10.1016/j.apcatb.2018.07.070
26. Kumarasamy K, Shah RG, Sundaradoss MV, Balu SK, Ramachandran R, Goud BN (2022) Analytical approach on Indian bentonites from Rajasthan: structural and physical characterization. Materials Today: Proceedings 64:549–553. https://doi.org/10.1016/j.matpr.2022.05.111
27. Bendou S, Amrani M (2014) Effect of hydrochloric acid on the structural of sodic-bentonite clay. J Min Mater Character Eng 2(September):404–413. https://doi.org/10.4236/jmmce.2014.25045
28. Kumar A, Lingfa P (2020) Sodium bentonite and kaolin clays: comparative study on their FT-IR, XRF, and XRD. Materials Today: Proceedings 22:737–742. https://doi.org/10.1016/j.matpr.2019.10.037
29. Ye X, Shi X, Jin B, Zhong H, Jin F, Wang T (2021) Natural mineral bentonite as catalyst for efficient isomerization of biomass-derived glucose to fructose in water. Sci Total Environ 778:146276. https://doi.org/10.1016/j.scitotenv.2021.146276
30. Al-essa, K. (2018). Activation of Jordanian bentonite by hydrochloric acid and its potential for olive mill wastewater enhanced treatment. J Chem, 2018. https://doi.org/10.1155/2018/8385692. Research
31. Djomgoue P, Njopwouo D (2013) FT-IR spectroscopy applied for surface clays characterization. J Surf Eng Mater Adv Tech 2013(October):275–282. https://doi.org/10.4236/jsemat.2013.34037
32. Mara, A., Wijaya, K., & Trisunaryati, W. (2017). Effect of sulfuric acid concentration of bentonite and calcination time of pillared bentonite effect of sulfuric acid concentration of bentonite and calcination time of pillared bentonite. The 3rd International Conference on Advanced Materials Science and Technology (ICAMST 2015), 020042(April 2016). https://doi.org/10.1063/1.4945496.
33. Nazdracheva T, Morozov A, Yavna V, Kochur A (2022) Study of hydration of kaolinite and montmorillonite mixture by IR spectroscopy. J Mol Struct 1250:131871. https://doi.org/10.1016/j.molstruc.2021.131871
34. De Oliveira CIR, Rocha MCG, Silva ALN, Bertolino LC (2016) Characterization of bentonite clays from Cubati, Paraíba (northeast of Brazil). Cerâmica 62:272–277. https://doi.org/10.1590/0366-69132016623631970
35. Baddour FG, Snowden-Swan L, Super JD, Van Allsburg KM (2018) Estimating precommercial heterogeneous catalyst price: a simple step-based method. Org Process Res Dev 22(12):1599–1605. https://doi.org/10.1021/acs.oprd.8b00245
36. Berraaouan D, Elmiz M, Essifi K, Salhi S, Tahani A (2020) Adsorption of carvacrol on modified bentonite in aqueous solutions. Materials Today: Proceedings 31:S28–S32. https://doi.org/10.1016/j.matpr.2020.05.280
37. Electricity Regulatory Authority and Consumer Protection Regulatory Authority,http://egyptera.org/ar/Tarrif6.aspx. Accessed in June 2019.
38. Gongyi Derui Machinery Co., Ltd,https://www.alibaba.com/product-detail/Wet-clay-rotary-dryer-for-drying_60536847731.html. Accessed in June 2019.
39. Henan Zhengzhou Mining Machinery Co., Ltd., https://www.alibaba.com/product-detail/Low-Price-Iron-Ore-Mill Grinding_1776706410.html?spm=a2700.7724857.normalList.208.60b72921l0CiHc. Accessed in June 2019.
40. Horizon Chemical for Special Chemicals Company,https://arabic.alibaba.com/product-detail/hydrochloric-acid-30-31-egypt-origin-industrial-grade-high-quality-50002375980.html. Accessed in June 2019.
41. Laizhou Taihe Chemical Machinery Co., Ltd, https://www.alibaba.com/product-detail/Multi-function-stirring-stainless-steel-reaction_60728476818.html?spm=a2700.details.maylikever.8.57e429a7QzzXSd. Accessed in June 2019.
42. ministry of housing ,utilities&Urban communities, https://www.hcww.com.eg/%D8%A3%D8%AD%D8%B3%D8%A8-%D9%81%D8%A7%D8%AA%D9%88%D8%B1%D8%AA%D9%83-%D8%A8%D9%86%D9%81%D8%B3%D9%83/, (Cited in June 2019).
43. Qixia Dali Mine Machinery Co., Ltd.,https://www.alibaba.com/product-detail/ball-mill-and-classifying-machine-MQGg_60820618267.html?spm=a2700.7724838.2017115.1.3fb15137zmYrLA&s=p. Accessed in June 2019.
44. Ro L, Novakovi T (2010) Modeling and optimization process parameters of acid activation of bentonite by response surface methodology. Appl Clay Sci 48(1–2):154–158. https://doi.org/10.1016/j.clay.2009.11.043
45. Thommes, M., Kaneko, K., Neimark, A. V, Olivier, J. P., Rodriguez-reinoso, F., Rouquerol, J., & Sing, K. S. W. (2015). Physisorption of gases , with special reference to the evaluation of surface area and pore size distribution (IUPAC Technical Report). https://doi.org/10.1515/pac-2014-1117.

46. Wuxi New Wuhuan Energy Saving Technology Co., Ltd,https://www.alibaba.com/product-detail/Longer-service-life-chiller-wenzhou-cooling_60824902758.html?spm=a2700.galleryofferlist.normalList.91.36381fccmtSuiJ&s=p. Accessed in June 2019.
47. Xiangtan County Centrifuge Plant Co., Ltd.,https://www.alibaba.com/product-detail/ISO-Certificate-Chemical-Industrial-Continuous-Flow_60606491283.html?spm=a2700.7724838.2017115.14.5a1a45b16Dzpp3&s=p. Accessed in June 2019.

Publisher's Note